Biochemical and Biophysical Research Communications 391 (2010) 664–668

Contents lists available at ScienceDirect

Biochemical and Biophysical Research Communications

journal homepage: www.elsevier.com/locate/ybbrc

The effect of Wag31 phosphorylation on the cells and the cell envelope fraction of wild-type and conditional mutants of *Mycobacterium smegmatis* studied by visible-wavelength Raman spectroscopy

Khozima Hamasha [a], Moodakare Bheema Sahana [a], Charul Jani [b], Seeta Nyayapathy [b], Choong-Min Kang [b], Steven J. Rehse [a,*]

[a] Department of Physics & Astronomy, Wayne State University, 666 W. Hancock, Detroit, MI 48201, USA
[b] Department of Biological Science, Wayne State University, 5047 Gullen Mall, Detroit, MI 48202, USA

ARTICLE INFO

Article history:
Received 3 November 2009
Available online 22 November 2009

Keywords:
Raman spectroscopy
Mycobacterium smegmatis
Phosphorylation
Peptidoglycan biosynthesis
Cell envelope fraction

ABSTRACT

Non-surface-enhanced Raman spectroscopy using a 514.5 nm wavelength laser has been used to measure the molecular difference of conditional mutants of *Mycobacterium smegmatis* expressing three different alleles: wild-type $wag31_{Mtb}$, phosphoablative $wag31T73A_{Mtb}$, and phosphomimetic $wag31T73E_{Mtb}$. This study demonstrates that the phosphorylation of Wag31, a key cell-division protein, causes significant differences in the quantity of amino acids associated with peptidoglycan precursor proteins and lipid II which are observable in the Raman spectra of these cells. Raman spectra were also acquired from the isolated P60 cell envelope fraction of the cells expressing $wag31T73A_{Mtb}$ and $wag31T73E_{Mtb}$. A significant number of the molecular vibrational differences observed in the cells were also observed in the cell envelope fraction, indicating that these differences are indeed localized in the cell envelope. Principal component analyses and discriminant function analyses were conducted on these data to demonstrate the ease of spectral classification and the reproducibility of the data.

Introduction

Tuberculosis (TB) is a worldwide health problem with a high mortality, infecting one out of every three people globally [1]. Latency, which creates a reservoir of persons with the potential to develop active tuberculosis, is especially important in the epidemiology and pathogenicity of tuberculosis. Despite its importance, it is still not clear how *Mycobacterium tuberculosis* controls the latent state in a human host [2]. However, to achieve, maintain, or escape from the latent state, *M. tuberculosis* must carefully regulate cell division, requiring a wide variety of signaling molecules.

Two protein kinases, PknA and PknB, are thought to be essential for signal transduction in this microorganism and have been shown to play an important role in regulating cell morphology and cell division [3–7]. Wag31, a substrate of PknA and PknB, is a homolog of the Gram-positive cell-division protein DivIVA that is localized in the cell poles in mycobacteria including *Mycobacterium smegmatis* and *Mycobacterium bovis* BCG, and controls cell morphology [8–10].

The phosphorylation of Wag31 plays a key role in the cell division of mycobacterium. We have previously shown that the expression of phosphomimetic *M. tuberculosis wag31* ($wag31T73E_{Mtb}$) in the *wag31* conditional mutant of *M. smegmatis* showed higher growth rate than cells expressing wild-type $wag31_{Mtb}$ or phosphoablative $wag31T73A_{Mtb}$ and that the phosphorylation of Wag31 regulates *M. smegmatis* peptidoglycan biosynthesis and growth of mycobacteria [10,11].

In this study, we observed molecular differences in the three *wag31* conditional mutants of *M. smegmatis* by using visible-wavelength Raman spectroscopy on the bacteria *in vitro*. Experiments performed on the P60 cell envelope fraction of these cells revealed similar spectroscopic differences.

Materials and methods

Microorganisms and growth conditions. The *M. smegmatis* conditional mutant strains of *wag31* containing tetracycline-inducible P_{tet}-*wag31*, P_{tet}-*wag31T73A*, or P_{tet}-*wag31T73E* at the *attB* locus were used in our study [10,12,13]. Cells were grown on 7H9-ADC agar plates containing 5 ng/ml tetracycline and 50 μg/ml hygromycin. Cells from the plate were inoculated in liquid 7H9 medium with 10 μg/ml hygromycin without inducer and cultured overnight to deplete the inducer and Wag31 inside the cells. Cells were reinoculated in 7H9-ADC liquid medium supplemented with 20 ng/ml tetracycline as an inducer followed by OD measurement every 3 h. *M. smegmatis* cells expressing *wag31WT*, *wag31T73A* and *wag31T73E* were harvested during log phase and washed once with

* Corresponding author. Fax: +1 313 577 3932.
E-mail address: rehse@wayne.edu (S.J. Rehse).

0006-291X/$ - see front matter © 2009 Elsevier Inc. All rights reserved.
doi:10.1016/j.bbrc.2009.11.117

1× phosphate buffer (137 mM NaCl, 2.7 mM KCl, and 11.9 mM phosphates) to remove traces of the media.

Cell envelope isolation. The cell envelope fraction (P60) was prepared as described in detail elsewhere [11]. The harvested cells with *wag31T73A* and *wag31T73E* allele were stored at −80 °C, then 8 g of harvested cells were resuspended in 30 ml of buffer A (50 mM MOPS (pH 8.0), 10 mM $MgCl_2$, and 5 mM β-mercaptoethanol) and subjected to probe sonication using 10 cycles of 60 s with 90 s cooling on ice between the cycles. The cell lysates were centrifuged at 23,000*g* (Beckman, JLA10.500) at 4 °C for 30 min. then the pellet was resuspended in buffer A and Percoll (GE Healthcare) was added to achieve a 60% final concentration. The resulting mixture was centrifuged at 23,000*g* for 60 min at 4 °C. The upper, flocculent band was recovered and washed with buffer A three times to remove residual Percoll. The pellet containing membranes and cell walls was then resuspended in buffer A using a Dounce homogenizer. The final concentrations of total protein from cells expressing *wag31T73E* and *wag31T73A* were 10 and 8 mg/ml, respectively.

Sample preparation. For Raman measurements on cells and cell envelope fractions, 10 μl of each of the suspensions was mounted onto a low-fluorescence quartz slide and dried in air prior to the Raman measurements. After each use the slides were cleaned with deionized water, acetone, and methanol successively to remove trace organic contaminants.

Raman spectroscopy. Raman measurements were performed with a Raman microscope system consisting of a Jobin–Yvon Horiba Triax 550 spectrometer, a liquid-nitrogen cooled charge-coupled device (CCD) detector, an Olympus model BX41 microscope using a 100× objective, and Innova 90 argon-ion laser (Coherent, Inc.) operating at 514.5 nm. The power at the sample was 10 mW. The Raman-scattered light from the sample was collected with the same microscope objective and focused on the entrance slit of a spectrometer with a 1200 line/mm diffraction grating. A notch filter placed in the scattered light path blocked all Rayleigh scattered 514.5 nm laser light. A PC running LabSpec software controlled the spectrometer and detector and recorded the spectra. Each spectrum was constructed from the average of three exposures with an exposure time of 10 s. Typically 10–20 spectra could be obtained from each dried 10 μl pad. Raman spectra were collected in the information-rich region between 600 and 2000 cm^{-1} with a spectral resolution of about 4 cm^{-1}. All Raman spectra were calibrated using Si as an external standard.

Spectral processing and data analysis. Background fluorescence in the Raman spectra was removed by a custom Matlab program utilizing an adaptive minmax method [14]. After fluorescence subtraction, the spectra were normalized by setting the maximum intensity to one. The Raman spectra were then analyzed using the multivariate chemometric techniques of principal component analysis (PCA) and discriminant function analysis (DFA) using SPSS data-analysis software (SPSS, Inc., v17.0). PCA is a well-known technique used to reduce the number of dimensions of data with a minimum loss of information by providing a set of principal components (PCs) which represent the original data. In this analysis PCA reduced the dimensionality of the spectra from 1993 channels to 13 PCs which were used as input independent variables into a DFA. DFA was used to discriminate between the different groups by maximizing the variance between the different groups and minimizing the variance within the same group.

Results and discussion

Raman spectra from bacterial cells

To ensure the reproducibility of the Raman spectra, approximately 100 spectra of each *M. smegmatis* mutant were obtained from suspensions of several cultures prepared over several weeks. Fig. 1 shows the average of the processed Raman spectra from cells expressing *wag31WT* (WT), *wag31T73A* (TA), and *wag31T73E* (TE). The spectra obtained from WT cells and TA cells are reproducibly similar while there are considerable differences between them and the spectra obtained from TE cells. The observed features in the Raman spectra reveal the composition of the bacterial cell, specifically protein, carbohydrates, lipid, and nucleic acids. The major peaks and their assignments are listed in Table S1. WT and TA spectra have significantly stronger protein peaks at 1518 cm^{-1} and at 1154 cm^{-1}, which have the assignments of carbon–carbon double bond and single bond stretching mode vibrations. TE has significant Raman features at 1310 cm^{-1}, which has previously been attributed to lipid vibrations; at 1361 and 1396 cm^{-1}, which have previously been attributed to D-glutamic acid, D-alanine, and *N*-acetylglucosamine; at 1448 and 1582 cm^{-1}, tentatively assigned to lipid vibrations; and at 1656 cm^{-1} which is a broad peak resulting from the overlapping of two peaks assigned for Amid I in protein and a carbon–carbon double bond stretching mode vibration in lipid.

The most statistically significant differences were revealed by performing the PCA on all of the spectra together. The original spectra consisted of 1993 intensity channels which the PCA was able to reduce into 13 principal components (PCs) which maintained 99.3% of the variance in the data sets. The first PC accounted for 70.9% of the data variation, while PC2 and PC3 accounted for 17.9% and 3.5%, respectively. A plot of PC loadings (shown in Fig. 2) provides significant information about the biochemical basis of the mathematical discrimination [15]. The loadings of PC1 are shown in Fig. 2A. This plot has strong negative peaks at 1154, 1518, and 1182 cm^{-1} (assigned to proteins) which are associated with the dominant features in the spectra from TA and WT cells.

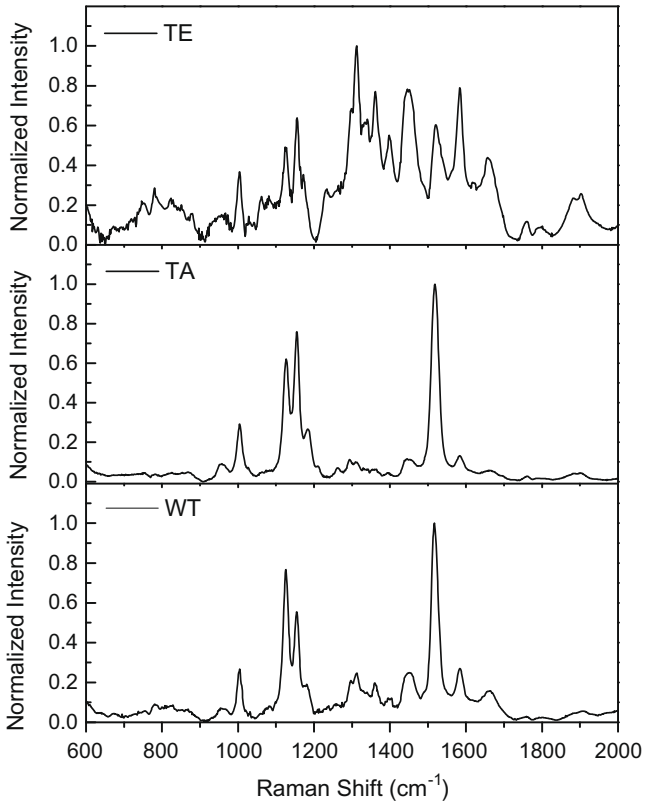

Fig. 1. Average Raman spectra of *M. smegmatis* expressing phosphomimetic *M. tuberculosis wag31* (*wag31T73E*$_{Mtb}$) (TE), wild-type *wag31*$_{Mtb}$ (WT), or phosphoablative *M. tuberculosis wag31* (*wag31T73A*$_{Mtb}$) (TA). Spectra were acquired with 514.5 nm laser excitation.

PC1 also has strong positive peaks associated with the dominant features in the spectra from TE cells, which were discussed above. This indicates that PC1 was constructed to maximize the spectral differences between TE cells and WT/TA cells and identifies the important biochemical components of these differences. PC1 does not show a considerable difference between TA and WT bacteria. To further highlight the significance of PC1, Fig. 2B shows a plot of PC1 and the resulting difference spectrum when the average spectrum of TA cells is subtracted from the average spectrum of TE cells and Fig. 2C shows a plot of PC1 and the resulting difference spectrum when the average spectrum of WT cells is subtracted from the average spectrum of TE cells. The similarities in these plots reinforce the interpretation that the basis of discrimination between spectra is the change in the Raman spectral features of the cells expressing phosphomimetic *wag31T73E*. It has been found that the third PC (PC3) is significant in the discrimination between TA and WT cells, based on the subtle differences in their spectra. Fig. 2D shows the similarity between the PC3 loadings plot and the resulting difference spectrum when the average spectrum of WT cells is subtracted from the average spectrum of TA cells. The main changes were observed in protein peaks at 1518, 1125, and 1154 cm^{-1}, although none of these are as large as the dominant features in 2B or 2C.

The 13 PC scores were used as independent input variables in a DFA which further reduced the dimensionality of the spectra. For discrimination among the three bacterial cell types, two discriminant function (DF) scores were calculated for each individual spectrum. The DFA allowed a rapid sorting or grouping of unknown spectra on the basis of the discriminant functions, and also gave an immediate measurement of the reproducibility of the spectra. In this analysis, 100% of the spectra obtained from the TE cells were correctly classified by the DFA in a leave-one-out classification test, indicating that these bacteria were reproducibly molecularly distinct from the other two groups. Only 69% of the TA bacteria and 88.9% of the WT bacteria were correctly classified, indicating that their spectra were similar to each other due to an almost identical molecular composition.

Raman spectra from bacterial cell envelope

In order to identify the changes present in the bacteria with the phosphomimetic form of Wag 31 and with the phosphoablative form of Wag31, the P60 cell envelope fraction was isolated and Raman measurements were performed on a dried suspension of the cell envelope. Fig. 3A shows the averaged Raman spectra for the P60 cell membrane fraction of bacteria with Wag31T73A (labeled "TA envelope") and with Wag31T73E (labeled "TE envelope"). Ninety-nine TA envelope spectra and 101 TE envelope spectra were averaged to make these spectra. Spectra of the P60 cell envelope fraction of the wild-type bacteria were not taken. Significant differ-

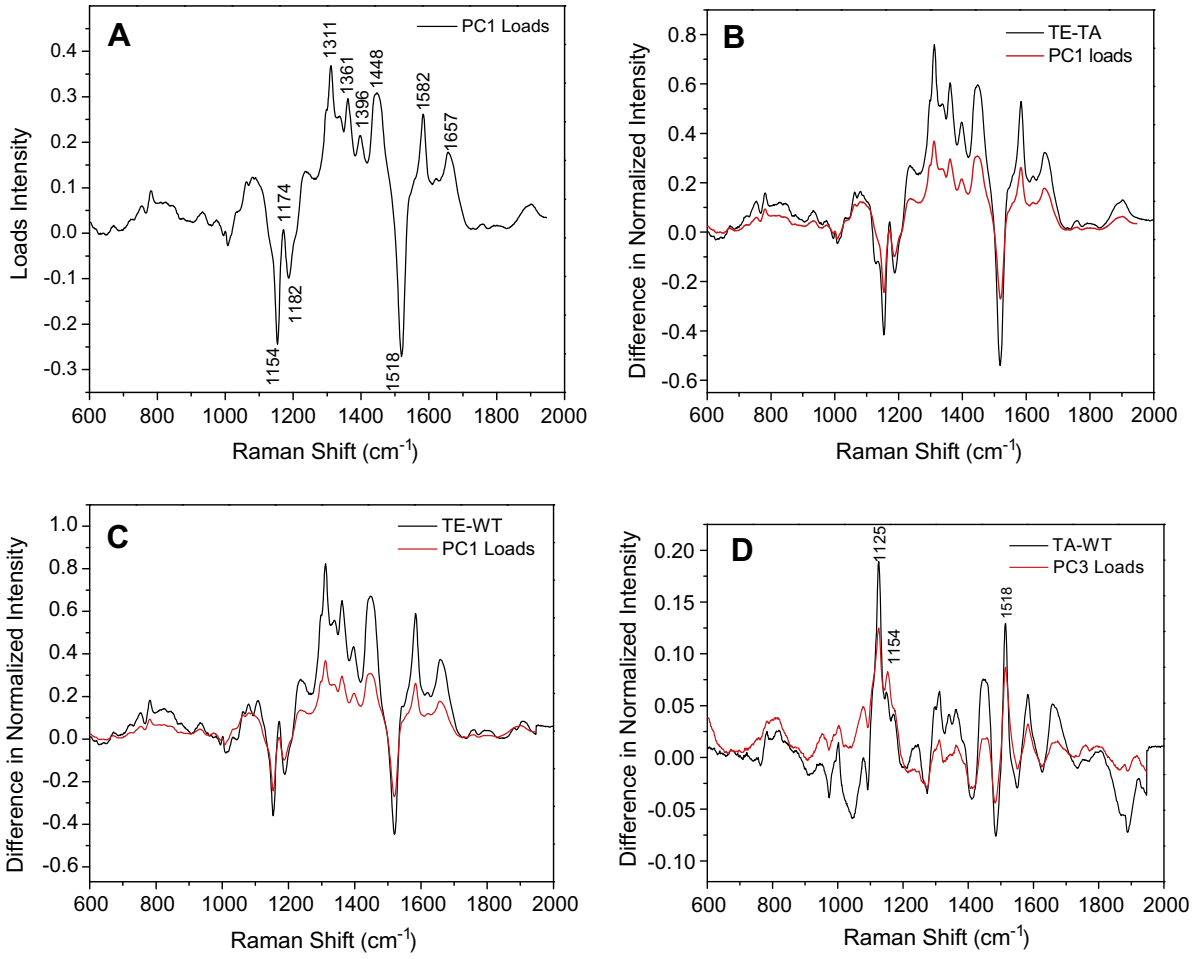

Fig. 2. Principal component loadings of the PCA performed on the Raman spectra acquired from three mutants of *M. smegmatis*. (A) The loadings of the first PC. Prominent spectral features are identified. (B) PC1 loadings plotted with the difference of the average Raman spectrum of TA cells and TE cells. (C) PC1 loadings plotted with the difference of the average Raman spectrum of WT cells and TE cells. (D) PC3 loadings plotted with the difference of the average Raman spectrum of TA bacteria and WT bacteria.

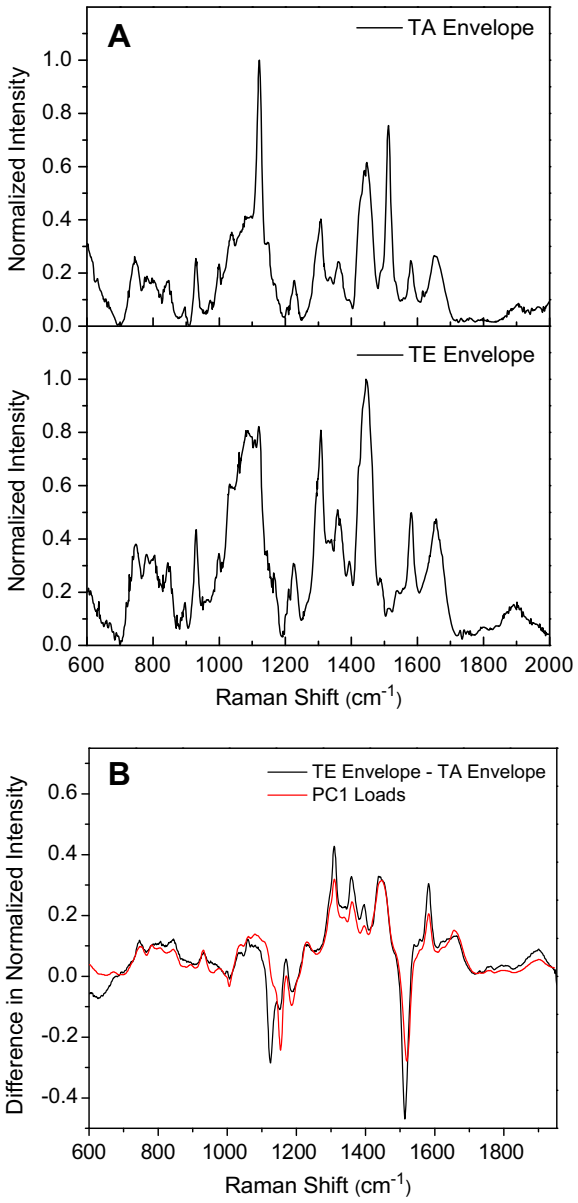

Fig. 3. Raman spectroscopy was performed on the P60 cell envelope fraction of the *M. smegmatis* cells expressing phosphoablative *wag31T73A*$_{Mtb}$ (TA) and phosphomimetic *M. tuberculosis wag31* (*wag31T73E*$_{Mtb}$) (TE). (A) The average Raman spectra of the TA and TE cell envelope fraction. (B) The difference between the average spectrum of the TA and TE cell envelope fraction plotted with the PC1 loadings.

ences between TA cell envelope and TE cell envelope can be observed at the same locations as were measured in the bacterial cells, indicating that significant cellular changes occurred in the cell envelope. Table S1 provides the detailed assignments for the main features which appeared in the cell envelope spectra. It was observed that the lipid peaks which are located at 1311, 1448, and 1582 cm^{-1} seem to be stronger in the TE envelope spectrum than in the TA envelope spectrum indicating that TE cell envelope contains more lipid than the TA cell envelope. Moreover, TE envelope spectra show an enhancement in the peaks assigned for amino acids in protein such as the peaks at 1361 and 1396 cm^{-1}. This result is consistent with the results of a study which revealed a higher enzymatic activity of peptidoglycan biosynthetic pathway (MraY and MurG) and a greater production of lipid II in cells expressing *wag31T73E*$_{Mtb}$ than cells expressing *wag31*$_{Mtb}$ or *wag31T73A*$_{Mtb}$ [11]. These Raman spectroscopic results indicate that cells with the *wag31T73E*$_{Mtb}$ allele produce more peptidoglycan precursor molecules than those expressing *wag31*$_{Mtb}$ or *wag31T73A*$_{Mtb}$. To accentuate the differences in these spectra, in Fig. 3B the average spectrum of the TA cell envelope has been subtracted from the average spectrum of the TE cell envelope and plotted with the PC1 loading from a PCA performed on these data. This analysis demonstrates that the PCA classification of these data relies on the main spectral changes in the Raman spectra of the samples under investigation.

Fig. 4 summarizes all the data obtained in this Raman spectroscopic study. Fig. 4A compares the average spectrum of the bacteria cells with their corresponding average spectrum obtained from the cell envelope fraction. Noticeably, considerable differences are observed between the spectra obtained from cells possessing the phosphoablative Wag31T73A and cells possessing the phosphomimetic Wag31T73E. Strong similarities (with some slight differences) in the spectra obtained from bacterial cells and the spectra obtained from the corresponding bacterial cell envelope indicate that the significant spectral changes observed between cells with Wag31T73A and Wag31T73E are primarily due to bio-

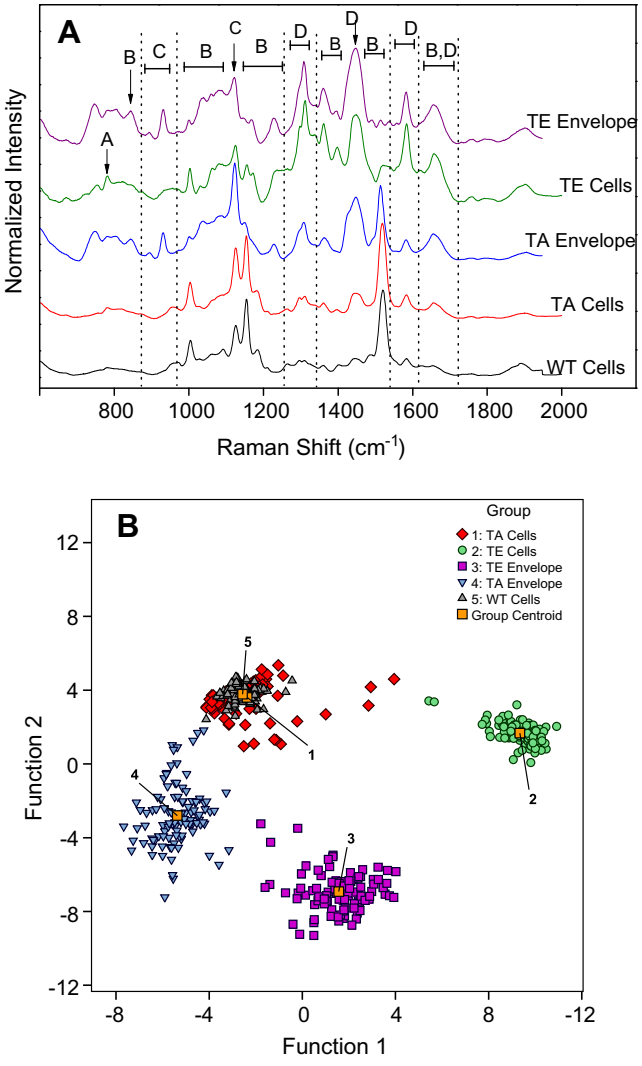

Fig. 4. A comparison of the average Raman spectra of the five classification groups studied in this work. (A) The Raman spectra of the cells of the three *wag31* conditional mutants of *M. smegmatis* and the spectra of the cell envelope fraction of two of them. (B) A PCA–DFA plot of all the Raman spectra showing the high-degree of similarity between WT and TA cells, and the ability to easily distinguish spectra from other groups.

chemical changes localized in the cell membrane and wall. Molecular identification of these differences suggests an increase in peptidoglycan biosynthesis and production of lipid II. These results are consistent with previous enzymatic studies and reports of the differences observed in cell-division and multiplication between cells with the $wag31T73E_{Mtb}$ allele and those expressing $wag31_{Mtb}$ or $wag31T73A_{Mt}$. Raman spectra from cells expressing $wag31_{Mtb}$ or $wag31T73A_{Mt}$ were almost identical. Fig. 4A shows the regions of the tentative assignments corresponding to the main components of the bacterial cells, namely, nucleic acids (A), proteins (B), carbohydrates (C), and lipids (D).

All the 516 spectra obtained from the five different samples (TE cell and envelope fraction, TA cell and envelope fraction, and WT cells) were analyzed using PCA followed by a DFA. The analysis resulted in the 100% correct classification of TE bacterial cell spectra, 99% correct classification of TE cell envelope spectra, 95% correct classification of TA cell envelope spectra, 67% correct classification of TA bacterial cell spectra, and 85.5% correct classification of WT bacterial cell spectra. The resulting PC-DFA plot (Fig. 4B) shows the first two computed discriminant function (DF) scores for all the Raman spectra obtained in this study. In this plot, each data point represents an entire spectrum. The highly similar spectra from the TA and WT cells are indicted by the overlapping of their clusters (points with similar DF1 and DF2 scores) in the DF plot. The between-group separation seen in Fig. 4B is caused by real biomolecular differences measured in the Raman spectra and demonstrates the ability of non-surface-enhanced visible-wavelength Raman spectroscopy to reveal subtle molecular differences in bacterial cells expressing different alleles and to localize those molecular differences in a specific domain of the cell structure. The clustering of data points around the group centroid in this graph which is composed of hundreds of spectra acquired from multiple cultures over an extended period of time also demonstrates that there is little variation in day-to-day measurements within the same group. The residual scatter in the data is indicative of typical measurement noise and is relatively small for similar studies of this nature. This DFA plot is a statistical chemometric way of quantifying the similarities and dissimilarities between the average spectra shown in Fig. 4A.

The results presented here demonstrate that visible-wavelength Raman-spectroscopy can be an effective tool to determine the biomolecular differences in the *wag31* conditional mutants of *M. smegmatis*, that this spectroscopy can be performed with excellent signal-to-noise on the cell envelope fraction of these cells, and that significant biochemical and/or structural changes in the cell envelope can be measured, indicating that *wag31* and its phosphorylation play an important role in peptidoglycan synthesis and the growth of mycobacteria.

Acknowledgments

The authors wish to gratefully acknowledge financial assistance from Mr. Richard Barber, as well as many helpful discussions on Raman spectroscopy with Dr. Vaman Naik and Dr. Ratna Naik.

Appendix A. Supplementary data

Supplementary data associated with this article can be found, in the online version, at doi:10.1016/j.bbrc.2009.11.117.

References

[1] 2007 Tuberculosis Facts Sheet, World Health Organization, 2007.
[2] A.A. Salyers, D.D. Whitt (Eds.), Bacterial Pathogenesis, a Molecular Approach, second ed., ASM Press, Washington, DC, 2002.
[3] P. Fernandez, B. Saint-Joanis, N. Barilone, M. Jackson, B. Gicquel, S.T. Cole, P.M. Alzari, The Ser/Thr protein kinase PknB is essential for sustaining mycobacterial growth, J. Bacteriol. 188 (2006) 7778–7784.
[4] C.M. Sassetti, D.H. Boyd, E.J. Rubin, Genes required for mycobacterial growth defined by high density mutagenesis, Mol. Microbiol. 48 (2003) 77–84.
[5] Y. Av-Gay, M. Everett, The eukaryotic-like Ser/Thr protein kinases of *Mycobacterium tuberculosis*, Trends Microbiol. 8 (2000) 238–244.
[6] S.T. Cole, R. Brosch, J. Parkhill, T. Garnier, C. Churcher, D. Harris, S.V. Gordon, K. Eiglmeier, S. Gas, C.E. Barry 3rd, F. Tekaia, K. Badcock, D. Basham, D. Brown, T. Chillingworth, R. Connor, R. Davies, K. Devlin, T. Feltwell, S. Gentles, N. Hamlin, S. Holroyd, T. Hornsby, K. Jagels, B.G. Barrell, et al., Deciphering the biology of *Mycobacterium tuberculosis* from the complete genome sequence, Nature 393 (1998) 537–544.
[7] C.M. Kang, D.W. Abbott, S.T. Park, C.C. Dascher, L.C. Cantley, R.N. Husson, The *Mycobacterium tuberculosis* serine/threonine kinases PknA and PknB: substrate identification and regulation of cell shape, Genes Dev. 19 (2005) 1692–1704.
[8] J.H. Cha, G.C. Stewart, The divIVA minicell locus of *Bacillus subtilis*, J. Bacteriol. 179 (1997) 1671–1683.
[9] K. Flardh, Essential role of DivIVA in polar growth and morphogenesis in *Streptomyces coelicolor* A3(2), Mol. Microbiol. 49 (2003) 1523–1536.
[10] C.M. Kang, S. Nyayapathy, J.Y. Lee, J.W. Suh, R.N. Husson, Wag31, a homologue of the cell division protein DivIVA, regulates growth, morphology and polar cell wall synthesis in mycobacteria, Microbiology 154 (2008) 725–735.
[11] C. Jani, H. Eoh, K. Hamasha, M.B. Sahana, M. Zeng, S. Nyayapathy, J.-Y. Lee, W. Suh, S.J. Rehse, D. Crick, C.-M. Kang, Regulation of polar peptidoglycan biosynthesis by Wag31 in mycobacteria, manuscript in preparation.
[12] C.A. Pashley, T. Parish, Efficient switching of mycobacteriophage L5-based integrating plasmids in *Mycobacterium tuberculosis*, FEMS Microbiol. Lett. 229 (2003) 211–215.
[13] M.C. Blokpoel, H.N. Murphy, R. O'Toole, S. Wiles, E.S. Runn, G.R. Stewart, D.B. Young, B.D. Robertson, Tetracycline-inducible gene regulation in mycobacteria, Nucleic Acids Res. 33 (2005). e221–7.
[14] A. Cao, A.K. Pandya, G.K. Serhatkulu, R.E. Weber, H. Dai, J.S. Thakur, V.M. Naik, R. Naik, G.W. Auner, R. Rabah, D.C. Freeman, A robust method for automated background subtraction of tissue fluorescence, J. Raman Spectrosc. 38 (2007) 1199–1205.
[15] A.S. Haka, K.E. Shafer-Peltier, M. Fitzmauurice, J. Crowe, R.R. Dasari, M.S. Feld, Identifying microcalcifications in benign and malignant breast lesions by probing differences in their chemical composition using Raman spectroscopy, Cancer Res. 62 (2002) 5375–5380.